

Nonlinear growth of magnetic islands by passing fast ions in NSTX

J Yang¹, E D Fredrickson¹, M Podestà¹ and F M Poli¹

¹ Princeton Plasma Physics Laboratory, Princeton, NJ 08543, USA

E-mail: jyang@pppl.gov

February 2022

Abstract. The growth of magnetic islands in NSTX is modeled successfully with the consideration of passing fast ions. It is shown that a good quantitative agreement between the simulation and the experimental measurement can be achieved when the uncompensated cross field current induced by passing fast ions is included in the island growth model. The fast ion parameters, along with other equilibrium parameters, are obtained self-consistently using the TRANSP code with the assumptions of “kick” model [Podestà *et al*, Plasma Phys. Control. Fusion **59** 095008 (2017)]. The results show that fast ions can contribute to overcoming the stabilizing effect of polarization current for the magnetic island growth.

Keywords: fast ions, Neoclassical tearing modes, Kick model, NSTX

Submitted to: *Plasma Phys. Control. Fusion*

1. Introduction

Neoclassical tearing modes (NTMs) cause formation of helical magnetic island structures that leads to a degradation of both thermal [1] and fast [2] ion confinement. The terms magnetic islands and NTM are often used interchangeably, in which cases NTMs mean magnetic islands formed by NTMs. The fast ion transport induced by NTMs have been successfully modeled in DIII-D [3] and NSTX [4] tokamaks.

Fast ions can affect NTMs. Theoretically, fast ions can affect the NTM rotation frequency [5], which qualitatively explains the NTM frequency “chirping” in correlation with bursts of fast ion losses as observed in ASDEX [6] and TFTR [7]. In another theory, however, fast ions can affect the NTM growth rate via formation of parallel current that alters either bootstrap [8] or polarization [9] current. This theory is yet to be tested experimentally: In a dedicated experiment in DIII-D, the change of fast ion distribution via modulated neutral beam (NB) injection was not correlated with a change of NTM width within the detection limit [10]. Other experiments in HL-2A [11], DIII-D [12],

and NSTX [4] did not focus on width or growth rate of NTMs. The difficulty in testing these theories stems from the difficulty in accurate experimental determination of fast ion and equilibrium parameters.

TRANSP [13] is a free-boundary equilibrium and transport solver, which can be operated using the “kick” model [14] to calculate the time evolution of fast ion and NTM parameters self-consistently. This framework was used for the analysis of fast ion transport induced by NTMs in DIII-D [3] and NSTX [4]. In this paper, we use the TRANSP framework to test the theories of fast ion effects on NTM growth rate, focusing on its effects on bootstrap current [9].

We assume that the single fluid approach is appropriate for NTM simulation, because the theories of fast ion effect on NTM we tested in this paper are developed using the single fluid model. An improved two fluid approach without fast ions [15] and a drift kinetic approach for fast ions [5] will be included in the future. We also assume that free parameters can be useful NTM simulation, not because the theory is inaccurate/overly simplified or the physics constants can change, but rather because of the measured quantities input to the model has uncertainties. This assumption, however, may also be useful in determination whether the existing NTM model can be applied to the shaped plasma equilibria.

This paper is organized as follows. The model used to simulate the magnetic island width time evolution is reviewed in Sec. 2. The experimental setup and the method to determine each parameters are presented in Sec. 3. The comparison of simulation and experiment is presented in Sec. 4. In Sec. 5, the results of numerical scan of NTM amplitude are discussed along with the simulated power transfer between fast ions and magnetic islands. Conclusion and future work can be found in Sec. 6.

2. Modified Rutherford equation augmented with fast ion term

In this section, the single fluid model for the magnetic island growth is presented, before the contribution of fast ions is introduced.

2.1. NTM physics

It is useful to consider the modified Rutherford equation [16] that governs the time evolution of island full width $w(t)$, or the NTM growth. In this paper, we adopt a dimensionless form:

$$\frac{1}{k_3} \frac{\tau_R}{r} \frac{dw}{dt} = [\Delta'_{m,n} + k_1 \Delta'_{NC} + k_2 \Delta'_{pol} + k_4 \Delta'_{GGJ}] r \quad (1)$$

where $\tau_R \equiv \mu_0 a^2 / \eta$ is resistive time scale where a is plasma minor radius, μ_0 is vacuum magnetic permeability and η is plasma resistivity, $r \leq a$ is minor radius at $q = m/n$ surface where m and n are toroidal and poloidal mode numbers, and k_1 – k_5 are free parameters of order unity (k_5 will be introduced later, see Eq. 4). The free parameters are included to account for the uncertainty in experimental determination of the input parameters.

The left hand side of Eq. 1 accounts for the effect of plasma resistivity on the island growth. The free parameter $1/k_3$ is 1.22^{-1} [17], subject to measurement uncertainties in the calculation of resistive diffusion time.

The first term in the right hand side of Eq. 1 is the classical stability index [18], which accounts for the effect of current and q profile shapes outside the tearing boundary region:

$$\Delta'_{m,n} = \left(\frac{\partial\psi^-}{\partial r} - \frac{\partial\psi^+}{\partial r} \right) / \psi |_{r=r_s}, \quad (2)$$

where $\psi = \psi_0 + \psi_{m,n}$ is the sum of equilibrium helical flux function

$$\psi_0(r) = (B_0/R_0) \int_0^r (1/q(r) - n/m)rdr$$

and the perturbed helical flux function $\psi_{m,n}$ which is the solution of the tearing mode equation

$$[\partial^2/\partial r^2 + 1/r\partial/\partial r - m^2/r^2 - (\partial J_0/\partial r)/(\partial\psi_0/\partial r)]\psi_{m,n} = 0,$$

r_s is location of $q = m/n$ surface, and the superscripts $-$ and $+$ denote integration outward from axis to island inner boundary and integration inward from wall to island outer boundary.

The quasi-cylindrical tearing mode equation is used. The radial cylindrical coordinate is related to normalized flux by the integral of $1/q - n/m$ over the radius. Both current and q profiles are taken from TRANSP, and they are not related by the simple cylindrical expression. The boundary conditions are zero on axis, matching at inner and outer edge of the island, and matching the conducting “wall” at $r_W/a = 1.24$. The resistive wall correction by electromagnetic drag is considered [19], and the assumed resistive wall time is 10 ms for a $n = 1$ perturbation. Single tearing mode layer is assumed.

The second term in the right hand side of Eq. 1 is the neoclassical drive (Equation (6) in [16]), which accounts for the loss of bootstrap current due to the flattened pressure gradient inside the island:

$$\Delta'_{NC} = \frac{16J_{BS}}{s < J > w^2 + w_d^2}, \quad (3)$$

where J_{BS} is bootstrap current, $s \equiv rq'/q$ is magnetic shear where prime denotes radial derivative, J is average current density for the region $0 < r < r_s$. The term w_d is a parameter which measures the extent to which cross-field transport can support a parallel temperature or density gradient (Equation (27) in [20]), which accounts for the preservation of pressure gradient in small islands where parallel transport becomes less effective:

$$w_d = k_5 \frac{r_s}{\sqrt{\epsilon sn}} \left(\frac{\chi_\perp}{\chi_\parallel} \right)^{1/4}, \quad (4)$$

where ϵ is magnetic inverse aspect ratio (see Sec. 3) and χ is electron thermal diffusivity with directions denoted as \perp (perpendicular to the magnetic field) and \parallel (parallel to the magnetic field).

We chose not to simplify this term to $\Delta'_{NC} \propto \sqrt{\epsilon}\beta_\theta$ where β_θ is thermal ion poloidal beta because the evolution of density and temperature gradients are not the same as the evolution of poloidal beta [16]. We chose not to expand this term to separately account for the contributions of density and temperature gradients to the bootstrap current [21] either, at least in this paper, to keep the number of free parameters to a minimum.

The free parameter k_1 is reported to range from 1.7 [22], 4.63 [21], 6.6 [16] to 9.2 [20] depending on the selection of neoclassical transport models. The free parameter k_5 is reported to range from 3.16 [21] to 5.1 [20]. In this paper, we take into account the measurement uncertainties of the input parameters including the transport coefficient using the free parameters.

The third term in the right hand side of Eq. 1 is the polarization current stabilization (modified from Equation (85) in [23], see Sec. 2.2 for the modification), which accounts for the polarization current induced by an electric field formed at a narrow layer surrounding the island separatrix due to difference in rotation velocities between an island and the surrounding plasma [24]:

$$\Delta'_{pol} = -\epsilon^{3/2} \frac{\rho_{\theta i}^2 \beta_\theta}{w^3} \left(\frac{L_q}{L_p}\right)^2, \quad (5)$$

where $\rho_{\theta i}$ is ion poloidal Larmor radius and $L_q \equiv q/\nabla q$ and $L_p \equiv p/\nabla p$ are gradient scale lengths of q and thermal pressure p .

We chose not to use an alternative expression involving electron beta instead of ion beta [21]. The dependence $\epsilon^{3/2}$ would be replaced by unity in a collisional plasma that features $\nu_i/\omega_* \ll 1$ where ν_i is ion collision frequency and ω_* is electron diamagnetic frequency. The free parameter k_2 is reported to range from 1.06 [24] to 1.64 [23].

Note that the polarization current stabilization term is inversely proportional to island width cubed, meaning the stabilization is more effective when the island is smaller. A special condition such as a drop of NTM frequency is needed for a small initial island to grow beyond the point where the polarization current stabilization is no longer effective, or to “open the gate” [25]. In Sec. 2.2, we will introduce another way to “open the gate”, which comes from fast ions.

The fourth term in the right hand side of Eq. 1 is the Glasser-Greene-Johnson or curvature stabilization effect (Equation (51) in [21]), which accounts for the bending of magnetic field lines by islands with finite plasma pressure [26, 27]:

$$\Delta'_{GGJ} = -\frac{\beta_\theta \epsilon^2 L_q^2}{r_s w |L_p|} \frac{q^2 - 1}{q^2}. \quad (6)$$

We chose to keep this form of curvature stabilization term in spherical tori based on the analysis shown in Fig. 8 of [28]. The free parameter k_4 is reported to range from 5.4 [21] to 6.3 [29].

Here, it is useful to remind that the values of free parameters cited here vary due to different assumptions in the calculations, whereas the free parameters account for measurement uncertainties in this paper.

2.2. Fast ion contribution to NTM physics

It is theoretically suggested that fast ions can form a parallel current to replenish the lost bootstrap current and stabilize NTM [8]. However, when the fast ion orbit size is larger than the island width, the parallel current is expected to be small due to the orbit averaging because the response of energetic ions to perturbation in the island region is weakened, resulting in the reduction of the particle distribution deformation which is the source of parallel current [9]. A recent gyrokinetic particle simulation shows only a weak stabilizing effect of the parallel current in DIII-D conditions [30]. The poloidal Larmor radius of typical beam ions in NSTX is 15 cm.

On the other hand, the orbit averaging has another consequence: The fast ion $E \times B$ drift is significantly reduced by orbit averaging, resulting in an “uncompensated cross field current” that helps maintain charge neutrality [31]. Here, E is the electric field formed at a narrow layer surrounding the island separatrix. The contribution of drifts other than the ion $E \times B$ drift to the current drive is not considered because they depend on charge and mass, allowing for electron return currents to form, rendering induced current dependent on fast ion density, which is relatively low. For comparison, the orbit averaging of thermal ions would result in the “neoclassical polarization current” [24], which is assumed to be lumped with the polarization current in this paper.

The uncompensated cross field current can alter the polarization current, thereby affecting the NTM stability, which can be quantified from Equation (13) of [9]:

$$\Delta'_u = \frac{\beta_\theta}{w} \left(\frac{L_q}{L_p} \right)^2 \left(\frac{L_{n_i}}{L_{n_h}} \frac{n_h}{n_i} \right), \quad (7)$$

where subscript u denotes uncompensated cross field current, $L_{n_i} \equiv n_i / \nabla n_i$ and $L_{n_h} \equiv n_h / \nabla n_h$ are gradient scale lengths of thermal ion density n_i and fast ion density n_h .

Note the similarity of Eq. 7 to Eq. 5, which is natural because both terms concern the same electric field formed at the island separatrix. There are two notable differences: The sign is different, and the uncompensated cross field current drive term has a $(L_{n_i}/L_{n_h})(n_h/n_i)$ dependence whereas the polarization current stabilization term has a $\rho_{\theta i}^2/w^2$ dependence. The different sign can be understood from the full Δ'_{pol} and Δ'_u expressions (Equations (12) and (13) of [9]):

$$\Delta'_{pol} = -\epsilon^{3/2} \frac{\rho_{\theta i}^2 \beta_\theta}{w^3} \left(\frac{L_q}{L_p} \right)^2 \frac{\omega'(\omega' - \omega_{*i})}{\omega_{*e}^2}, \quad (8)$$

and

$$\Delta'_u = -\frac{\beta_\theta}{w} \left(\frac{L_q}{L_p} \right)^2 \left(\frac{L_{n_i}}{L_{n_h}} \frac{n_h}{n_i} \right) \frac{\omega'}{\omega_{*i}}, \quad (9)$$

where ω' is the island rotation frequency relative to plasma, and ω_{*i} and ω_{*e} are the ion and electron diamagnetic frequencies. Since it is difficult to measure the NTM frequency in plasma rest frame due to the typically much larger contribution from the Doppler shift caused by plasma rotation compared to the small signal, we assume that the NTM frequency is approximately the same as the electron diamagnetic frequency,

i.e., $\omega' \approx \omega_{*e} < 0$. We also assume that $\omega_{*i} \approx |\omega_{*e}|$. With such assumptions, Eq. 8 reduces to Eq. 5 as $\omega'(\omega' - \omega_{*i})/\omega_{*e}^2 \rightarrow 2$ (the factor 2 is included to k_2 subsequently), and Eq. 9 reduces to Eq. 7 as $\omega'/\omega_{*i} \rightarrow -1$.

Here, we adopted the theory that when $\omega' < 0$ or $\omega' > \omega_{*i}$, $\Delta'_{pol} < 0$ (stabilizing) [23]. As will be shown in Sec. 4, it is necessary that $\Delta'_u > 0$, i.e. the uncompensated cross field current drive NTM, competing against the stabilizing polarization current, to achieve a quantitative agreement between simulation and measurement in NSTX. Therefore, we assume $\omega' < 0$. If $\omega' > \omega_{*i} > 0$, both polarization current and uncompensated cross field current are stabilizing [9] and the simulation fails. Another theory that stems from the selection of a different potential profile is that $\Delta'_{pol} < 0$ only when $\omega' > 0$ [32]. The calculation of uncompensated cross field current for the potential profile selected in [32] is beyond the scope of this paper.

In its final form, the modified Rutherford equation (Eq. 1) retains its structure but the polarization current term (Eq. 5) now includes the fast ion contribution:

$$\Delta'_{pol} = -\epsilon^{3/2} \frac{\rho_{\theta i}^2 \beta_{\theta}}{w^3} \left(\frac{L_q}{L_p}\right)^2 + \frac{\beta_{\theta}}{w} \left(\frac{L_q}{L_p}\right)^2 \left(\frac{L_{n_i}}{L_{n_h}} \frac{n_h}{n_i}\right). \quad (10)$$

3. Experimental setup and determination of parameters

NSTX [33] is a spherical torus with major radius $R_0 = 0.85$ m, minor radius $r = 0.60$ m, toroidal field $B_{T0} \leq 0.55$ T, and plasma current $I_P \leq 1.5$ MA. NSTX discharge #134020 is in NB heated H-mode at $B_{T0} = 0.5$ T and $I_P = 1.0$ MA. At time $t = 0.7$ s, the central electron density $n_e = 1.0 \times 10^{20}$ m⁻³ and temperature $T_e = 0.8$ keV as measured by a Thomson scattering diagnostic [34], the central ion density $n_i = 0.7 \times 10^{20}$ m⁻³ and temperature $T_i = 0.8$ keV as derived by charge exchange spectroscopy (CHERS) [35], and the central fast ion density $n_h = 1.2 \times 10^{18}$ m⁻³ as calculated self-consistently with other measured parameters by TRANSP [13] (see Fig. 1). Note that the fast ion density profile is calculated assuming the “kick” model (to be introduced in the next paragraph) for the stability analysis presented in this paper. The safety factor is reconstructed from equilibrium reconstruction code LRDFIT [36] with constraints including those from motional Stark effect polarimetry (MSE) [37]. The $q = 2$ surface is located at normalized poloidal flux $\psi/\psi_a = 0.4$.

In NSTX #134020, a core non-resonant $n = 1$ kink mode typically accompanies a $(m, n) = (2, 1)$ NTM as it is typical in NSTX [38]. Note that the NB power is reduced to find the “marginal point” from which the small island effect can be studied experimentally [28]. The effect of these perturbations should be included to the analysis, as is shown in Fig. 2 that from 0.67–0.71 seconds, the measured and simulated neutron rates S_n diverge by around 10% when assuming the “classical” model, but agree within 5% when assuming the “kick” model [4]. The “kick” model is a physics-based, reduced fast ion transport module in TRANSP [13] originally developed to quantitatively analyze the effect of Alfvén eigenmode instabilities on fast ion transport [39]. The classical and “kick” models indicate the different physics included in TRANSP NUBEAM [40]

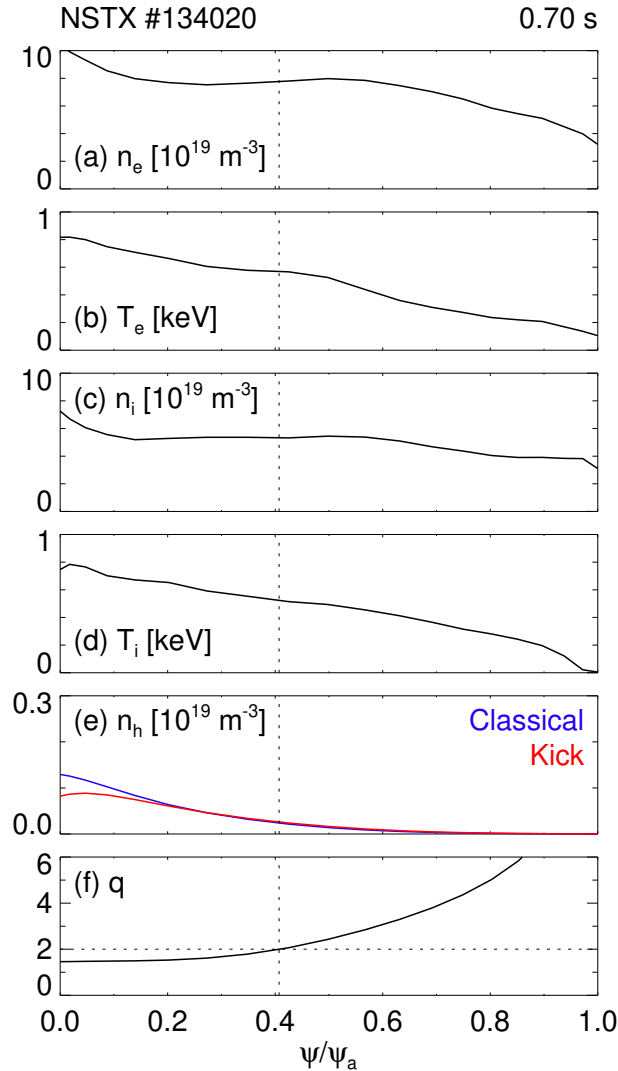


Figure 1. Profiles of (a) electron density, (b) electron temperature, (c) thermal ion density, (d) thermal ion temperature, (e) fast ion density, and (f) safety factor. For panel (e), colored lines indicate fast ion densities calculated assuming the classical model (blue) and the Kick model (red).

calculations, in that the classical model considers collisional scattering, slowing down, and atomic reactions, whereas the “kick” model considers the effect of perturbations in addition to those considered in the classical model. TRANSP is an integrated tokamak modeling code, and NUBEAM is a Monte Carlo fast ion module within TRANSP. A “kick” is the change in fast ion energy and momentum induced by the prescribed perturbations. The perturbation is input based on the mode parameters determined by a soft X-ray (SXR) diagnostics as in Fig. 3. The line-integrated SXR emissivity is forward-modeled using an analytic base function and compared to the measurement with mode parameters adjusted to minimize the difference the two [4]. Once the mode

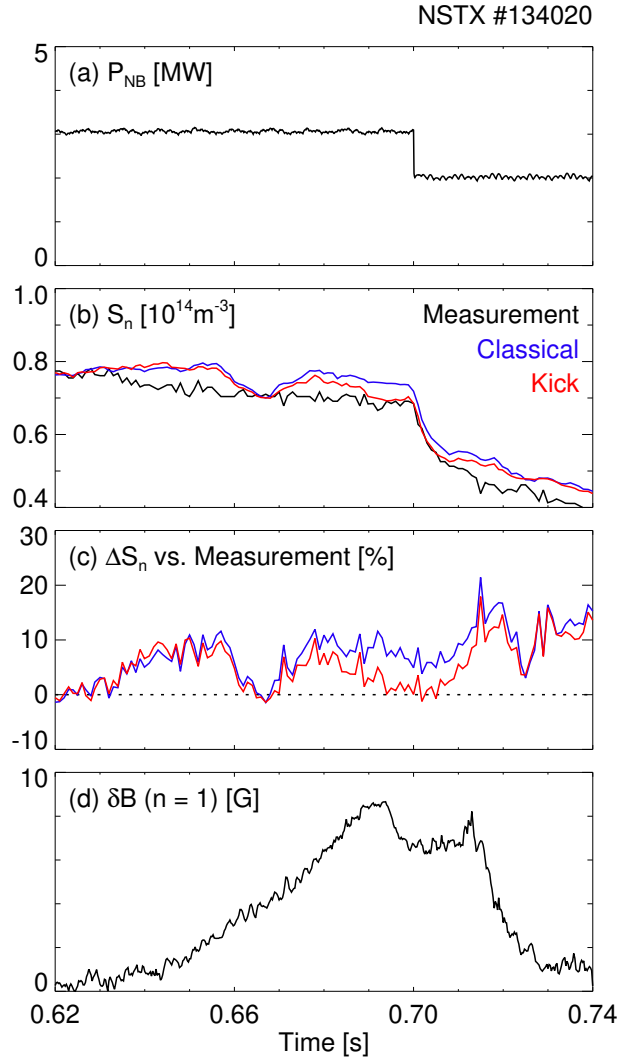


Figure 2. Time evolution of (a) neutral beam power, (b) neutron rate, (c) neutron rate difference with respect to the measurement, and (d) $n = 1$ mode amplitude. For panels (b) and (c), measurement is in black and simulation is in blue (classical model) and red (Kick model).

parameters are determined, the same analytic base function is used to provide an input to the Hamiltonian guiding center code ORBIT [41] to calculate the kick probability matrix, which is then input to TRANSP. The fact that the “kick” model successfully reproduces the measured neutron rate as shown in Fig. 2 indicates that both “kick” model and SXR measurement are valid to be used for the stability analysis.

The fast ion contribution to NTM stability depends on the gradient scale length of thermal ion density L_{n_i} . We use n_i derived from CHERS, which is prone to uncertainties: CHERS actually measures the intensity of a specific carbon emission line, from which the carbon density is inferred; n_i is then derived from the carbon density profile and an

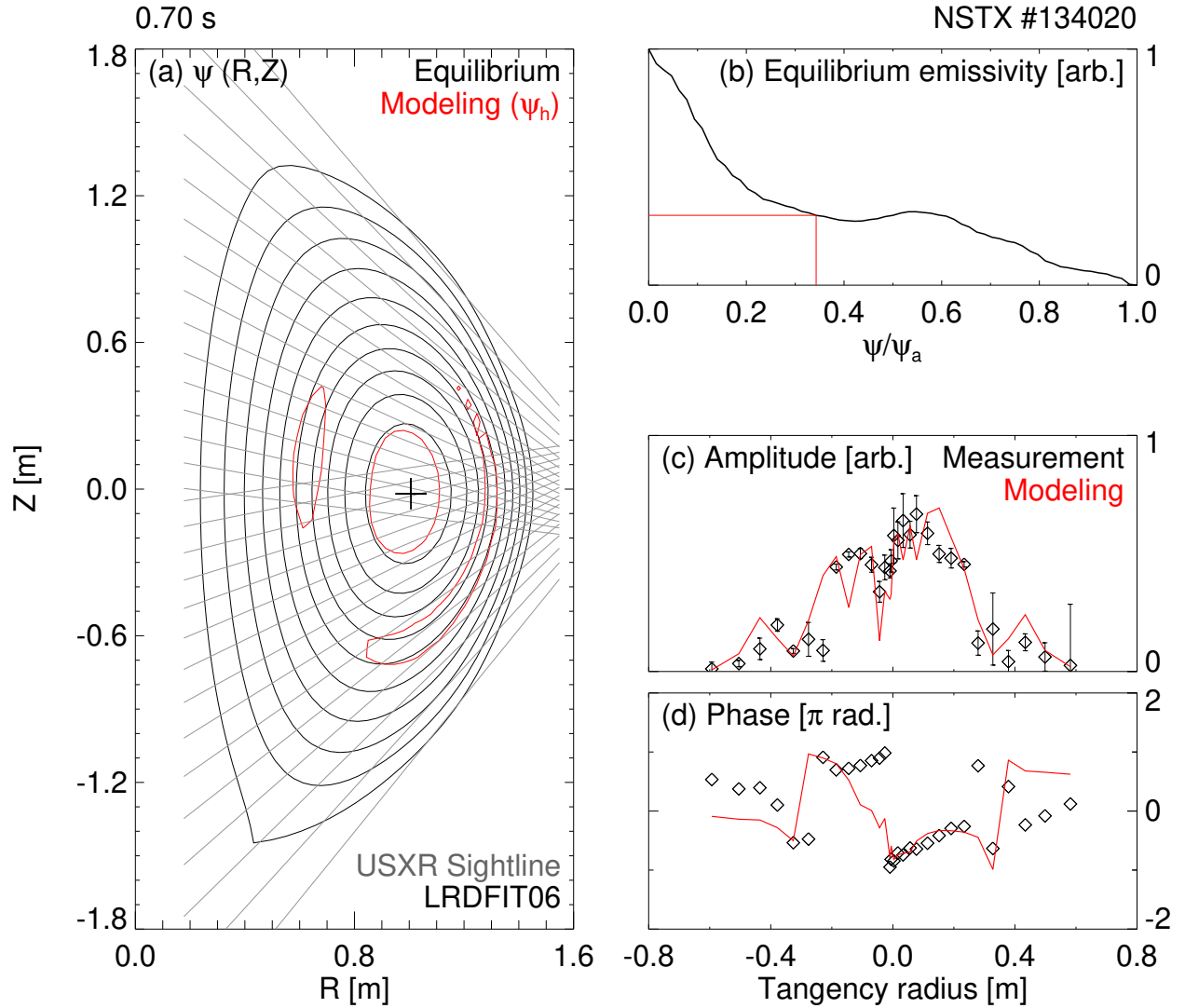


Figure 3. (a) Contour of equilibrium flux surfaces (black) and modeled island boundaries (red) overlaid with SXR sightlines (gray); (b) Profile of equilibrium emissivity with $q = 2$ surface highlighted; Plot of (c) amplitude and (d) phase at each SXR diagnostic channel shown in tangency radii of the respective channel.

additional input of Z_{eff} , which requires n_i to calculate \ddagger . The validity of measured n_i can be tested using TRANSP (Fig. 4). For CHERS, we assumed $n_i = n_C + n_D$ where C and D denote carbon and deuterium. For TRANSP, n_i is calculated along with other parameters self-consistently based on quasi-neutrality. It is shown that n_i measured by CHERS and calculated by TRANSP are in good agreement near $q = 2$ surface, indicating that the data from CHERS are consistent with other diagnostics, such as Thomson scattering diagnostic near the $q = 2$ surface. It is also seen in Fig. 4 that

\ddagger The Z_{eff} profile is calculated using CHERS with the assumption that carbon is a dominant impurity in NSTX

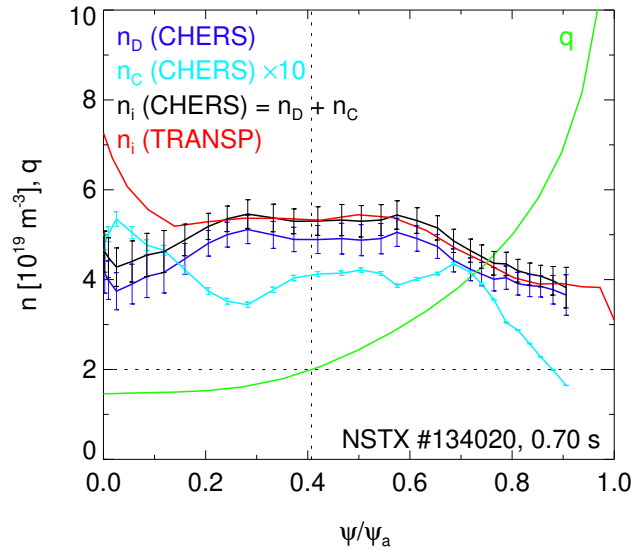


Figure 4. Comparison of ion density profiles from CHERS (total in black, Deuterium component in blue, Carbon component in cyan) and TRANSP (red). Safety factor profile is shown in green for reference.

near the core, the CHERS and TRANSP n_i diverge, which indicates that either one of CHERS and TRANSP or both may be inaccurate there. However, this is not of interest in this paper because the fast ion contribution to stability need to be calculated at the $q = 2$ surface, not at the core. It is still valuable to discuss the possible reason of this divergence to better understand the TRANSP calculation procedure: As a discharge approaches its end, there is typically an accumulation of carbon near the core, which causes the electron density to increase, leading to the increased ion density during the transport calculations in TRANSP.

Terms related to small island effect, Eqs. 4–6, includes aspect ratio ϵ . Rigorously, toroidal effects that ϵ represents come from the variation in total B , that is, $\epsilon_B \equiv (B_{in} - B_{out}) / (B_{in} + B_{out})$, instead of the geometric aspect ratio $\epsilon = a/R$ [28]. In spherical tori like NSTX, the two parameters can be different as shown in Fig. 5 (a). Therefore, we use ϵ_B in this paper.

The neoclassical drive term, Eq. 3, includes bootstrap current J_{BS} and total current J . TRANSP NCLASS [42] module is used to calculate these parameters as shown in Fig. 5 (b).

All terms in Eq. 1 include q profile. MSE-LRDFIT is used to determine the q profile, with additional constraints provided by CHERS and Mirnov spectroscopy: The toroidal rotation frequency of the plasma measured by CHERS and the NTM frequency measured by Mirnov coil spectroscopy are compared to determine the mode rational surface location, assuming the islands rotate at approximately the same frequency as the plasma. The MSE-LRDFIT q profile is shifted to match the new location of mode rational surface while mostly maintaining the magnetic shear (Equation (3) in [43]), as shown in Fig. 5 (c). We chose to maintaining the magnetic shear because LRDFIT

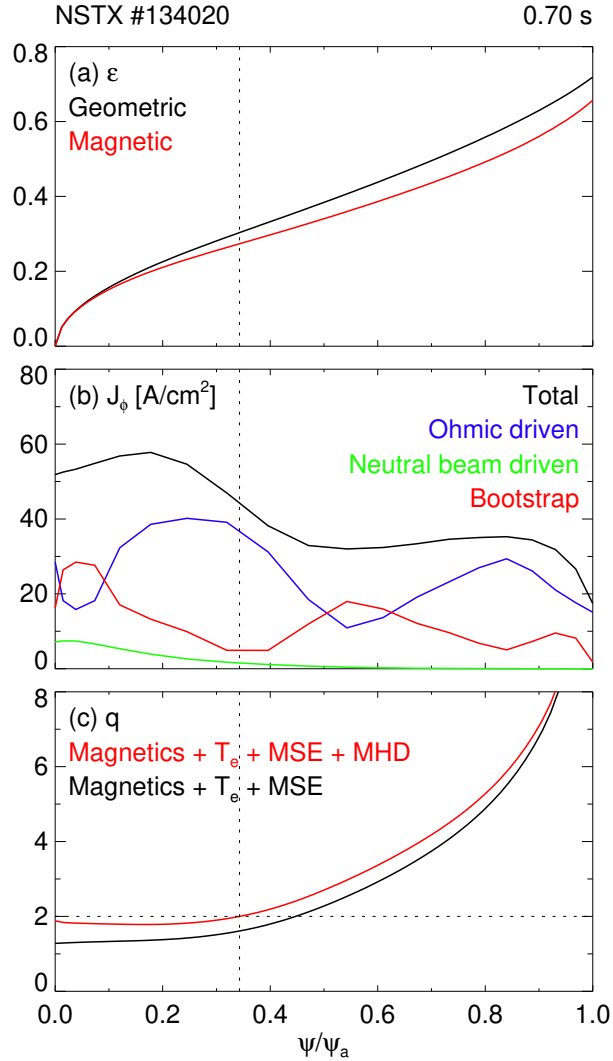


Figure 5. Profiles of (a) magnetic (red) and geometric (black) inverse aspect ratio, (b) TRANSP current profiles, and (c) magnetohydrodynamic (MHD) mode constrained (red) and MSE constrained (black) safety factor. For panel (b), total current is in black, Ohmic and neutral beam driven currents are in blue and green, and bootstrap current is in red.

tends to preserve the shape of the pitch angle profile while shifting the entire profile to match the measured plasma current I_P .

4. Comparison of simulation and experiment

In this section, the quantitative test of the fast ion contribution described in Sec. 2.2 is presented. The time evolution of magnetic island width is modeled using the modified Rutherford equation (Eq. 1) with each term described in Eqs. 2, 3, 4, 6, 10 in Secs. 2.1 and 2.2. The fitting procedure is introduced, before the simulation results are presented

and discussed.

4.1. Multi-parameter least squares fit

A multi-parameter least squares fit algorithm, also known as Levenberg-Marquadt algorithm [44], is used to determine the coefficients k_1 – k_5 and the initial value of the island width. The unknowns are scaled to be the order of unity, limited at [0,10]. The island width values at each time slice are used as constraints, typically at 1 ms interval, the order of 10^2 constraints. The weight of constraints at the island growth phase are set at values ten times larger than those at the island shrinking phase since the modified Rutherford equation is known to be more accurate in the island growth phase.

The initial guess of the unknowns are provided by the user, and the algorithm *tries* to find the global minimum in $\chi^2 \equiv \sum((y_i - p_i)^2 \times |u_i|)$, where y_i , p_i and u_i are i-th constraint, projection, and weight, on a six-dimensional parameter space of unknowns (with range in each dimension being [0,10]). Often the algorithm fails to find the global minimum because of a local minimum: If a fit result is a local minimum, it is only valid for the small subset of initial guess of unknowns. The sensitivity study (Sec. 4.3) is useful to determine if the fit is a global or local minimum.

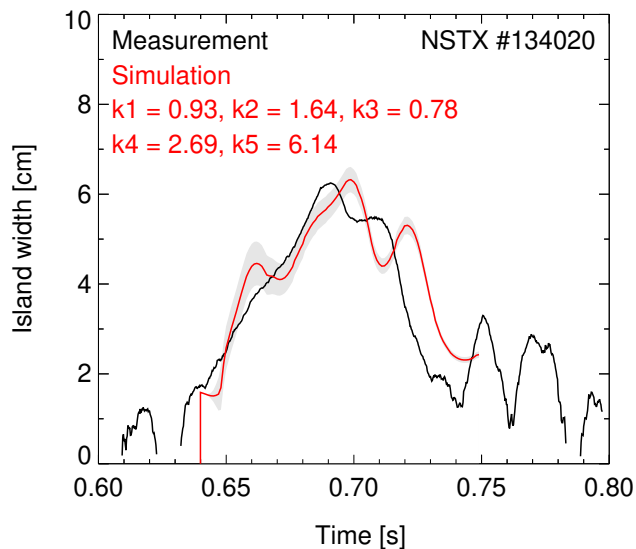


Figure 6. Comparison of measured (black) and simulated (red) island width time evolution. The shaded area indicates the error bar of the simulation. Modified Rutherford equation coefficients k_1 – k_5 are also shown.

4.2. Simulation

The quantitative test of the fast ion contribution described in Sec. 2.2 is shown in Fig. 6. The values of coefficients k_1 – k_5 are within orders of the expected range described in Sec. 2.1. The error bar indicated by shaded area indicates the effects of fit variance in

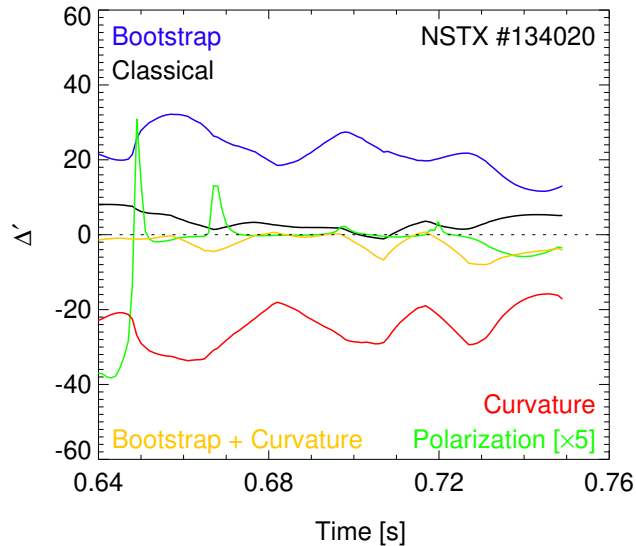


Figure 7. Comparison of classical (black), bootstrap current (blue), polarization current (green) and curvature (red) effect on NTM stability. Note that Δ'_{pol} is amplified 5 times for the visual aid.

each parameter. The sensitivity study presented in Sec. 4.3 shows that the fit result shown here is a global minimum.

Since the numerical optimization ensures that the simulated and measured time evolution of the island widths converge, it is more interesting to analyze the individual terms that contribute to the simulation, as shown in Fig. 7. It is immediately noticed that the curvature stabilization (red) is as strong as the bootstrap current drive (blue). The main contribution of the island growth comes from the classical effect (black), since the polarization current effect (green) becomes insignificant as the island grows, and the sum of bootstrap current drive and curvature stabilization (yellow) remains small before it goes negative (curvature stabilization dominates bootstrap current drive) as the island shrinks. Note that in Fig. 6, it is shown that the island width grows like $w \sim t$, as would classical tearing modes, not like $w \sim t^{1/2}$, as would neoclassical tearing modes. In other words, we have found the evidence that a magnetic island may not necessarily be a “classical” tearing mode even if it grows like $w \sim t$, when the curvature term is sufficiently large as is often the case in spherical tori [28].

The effect of fast ions in the magnetic island growth phase is shown more clearly in Fig. 8, where the polarization current term (Eq. 10) is broken down to the fast ion part (Eq. 7) and the thermal ion part (Eq. 5). Notice that the total growth rate at the onset of the magnetic island is only marginally positive. Without the fast ion part that contributes to the growth of the magnetic island, the thermal ion part alone could not push the total growth rate above zero. In other words, when the fast ion part is omitted from the model, the simulation crashes ($w \rightarrow 0$) unless the free parameter for polarization current term, k_2 , is set at zero. It is therefore necessary to include the fast ion part to achieve a good quantitative agreement between the simulation and

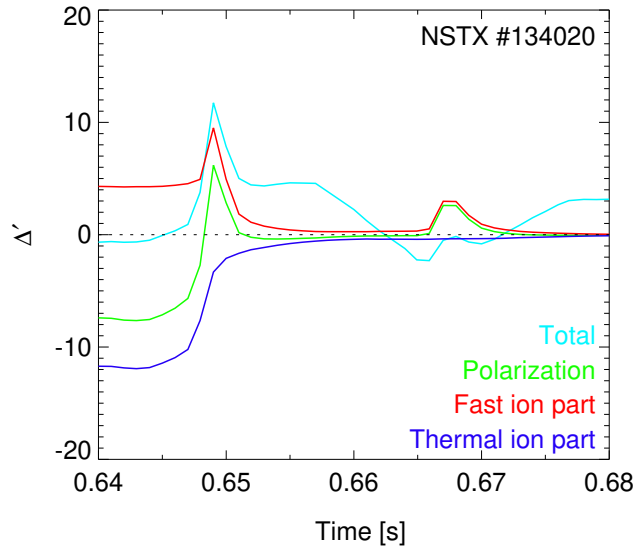


Figure 8. Redraw of Fig. 7 focusing on the island width growth phase (0.64–0.68 seconds). The polarization Δ'_{pol} (green) is the same as that of Fig. 7, except in Fig. 7 the value is amplified 5 times for the visual aid. The sum of fast ion Δ'_u (red) and thermal ion $\Delta'_{pol} - \Delta'_u$ (blue) part is the same as the polarization Δ'_{pol} (green). The total Δ' (cyan), not shown in Fig. 7, is shown here.

the experimental measurement. Also notable in Fig. 8 is that as the island grows, the thermal ion part of $\Delta'_{pol} \sim 1/w^3$ decreases faster than $\Delta'_u \sim 1/w$.

That the polarization current term is overly significant was previously reported [21]. That the addition of fast ion term allows finite k_2 could be the answer to this conundrum.

4.3. Sensitivity study

A multi-parameter fit may converge to a local minimum, not to the intended global minimum. To determine the nature of the convergence, a set of initial guess for the fit is taken randomly from the positive side of a Gaussian distribution between [0,10]. If the fit is a local minimum, the fit result will depend on the initial guess, whereas if the fit is the global minimum, the fit result will be independent of the initial guess. In a plot of fit results versus initial guesses, convergences to local minima will result in a “linear” response, whereas convergences to the global minimum will result in a “flat” response.

The sensitivity study for the results in Sec. 4.2 is shown in Fig. 9. Here, only the results with small $\chi^2 < 0.5$ are shown. For all parameters in Fig. 9, the response of fit result to initial guess is flat, indicating that the fit result in Fig. 6 is the global minimum.

Although not linear, the plot Fig. 9 (e) shows a larger variance in the fit result than in other plots. This implies that for k_5 , there is a large fit uncertainty although the fit is independent of the initial guess. This is plausible because unlike other free parameters shown in Eq. 1, k_5 is not directly related to the island width: It is buried in the expression of Δ'_{NC} as shown in Eqs. 3 and 4.

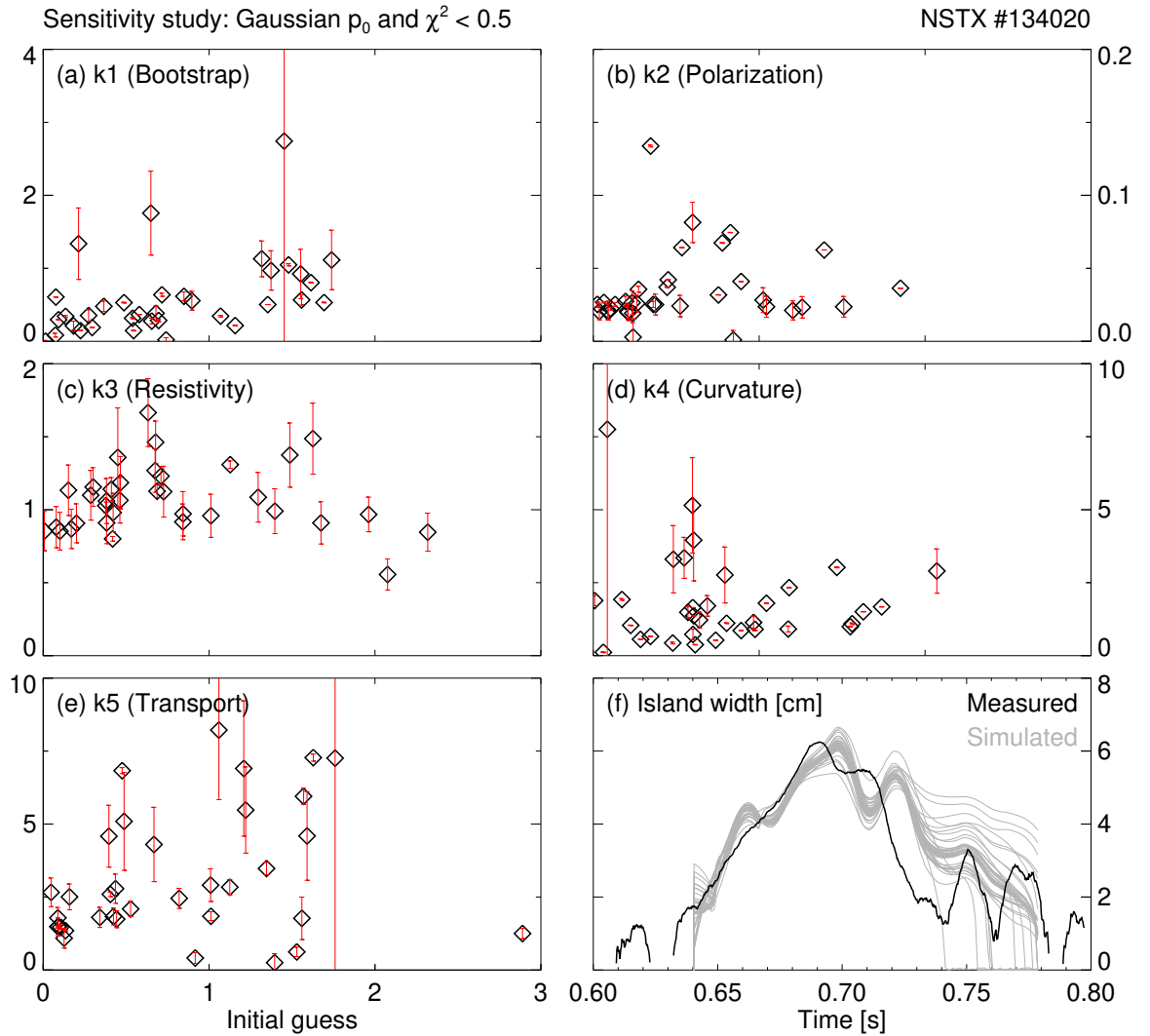


Figure 9. (a-e) Response of modified Rutherford equation coefficients k_1 – k_5 to changes in initial guess of each coefficients; (f) Comparison of measured (black) and simulated (gray) island width time evolution. Each point in (a-e) corresponds to a grey line in (f).

Note that in Fig. 9, the initial guesses of all parameters exceeding the value of 2 rarely survives the χ^2 test. This indicates that we may safely limit the initial guess further to $0 < k_i < 2$ for a faster convergence, if necessary.

4.4. Limitations of the model

Some physics are missing in the model presented in this paper. The parallel current effect induced by passing fast ions [8] may become significant as island grows larger to be comparable to the Larmor radius of typical beam ions in NSTX $\rho_{\theta i} \leq 15$ cm, but is not included in this paper. The possible dependence of neoclassical drive on

different bootstrap current sources [21] is also missing. The effect of island rotation, which affects not only the thermal but also fast ion contribution on NTM stability, is also left for future work.

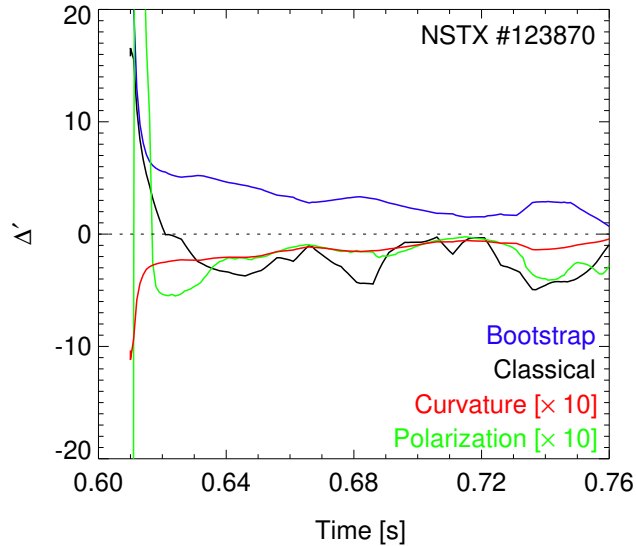


Figure 10. Same as Fig. 7, but for NSTX discharge #123870. Note that Δ'_{NC} and $\Delta'_{m,n}$ are amplified 10 times for the visual aid.

Some parts of the model can be improved. For some discharges as the one shown in Fig. 10, $\Delta'_{m,n}$ is calculated to be negative. In this circumstance, the fit produces large χ^2 and σ values unless the fast ion contribution becomes abnormally large to overcome the strong stabilizing factors, indicating that the model does not agree with the measurement. This can be interpreted as that the fit lacks a degree of freedom in driving terms needed to match the measurement. It is suggested that trapped fast ions may affect TM stability [45], which might be the reason why $\Delta'_{m,n}$ is *falsely* evaluated to be negative, especially in low magnetic shear plasmas such as NSTX as shown in Fig. 1. With the missing fast ion contribution on TM stability, the fits in these discharges can be improved. Another possible source of drive is the magnetic coupling of NTM with the nonresonant core kink mode, which rotates at the same frequency as NTM, but is not included in the analysis presented in this paper. A benchmark of $\Delta'_{m,n}$ evaluation will provide an improvement to the model.

5. Discussion

In this section, the results of qualitative analyses for the fast ion contribution discussed in Sec. 2.2 is presented.

In Fig. 11, the fraction of lost fast ions is seen to grow rapidly as the mode amplitude is numerically scanned beyond the measured mode amplitude. The fraction of lost fast ions is calculated using ORBIT as the input mode amplitude is numerically scanned from

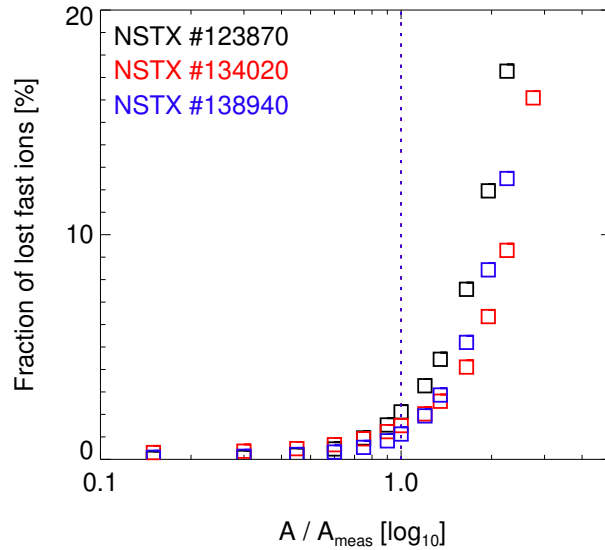


Figure 11. Plot of fraction of lost fast ions against mode amplitude normalized by measured mode amplitude. Three different discharges, NSTX #123870 (black), #134020 (red), and #138940 (blue) are shown.

$0.15\times$ to $2.75\times A_{meas}$, where A_{meas} is the measured mode amplitude that corresponds to the measured island width. The distinctively rapid growth of fast ion loss beyond a certain threshold is observed, and more interestingly, the threshold is at $A = A_{meas}$, in at least three discharges with different q profiles in NSTX.

One way of interpreting Fig. 11 is that a magnetic island stops growing when the fast ion transport starts to increase rapidly. It is almost as if the reduced number of fast ions due to the enhanced transport weakens the fast ion drive of NTM (see Eq. 7). In DIII-D, the increased fast ion transport has been observed, but the island was allowed to grow beyond the threshold for distinctively rapid growth of fast ion loss [3]. This difference may be attributed to the absence of core kink mode in DIII-D that accompanies NTM in NSTX, if the core kink mode and NTM are communicating with each other in terms of fast ion transport. This turns out to be true, as we will see in the next paragraph.

The energy exchange inside the flux surface from fast ions to the magnetohydrodynamic (MHD) modes is shown in Fig. 12 (a) and (b). Here, $P_{EP \rightarrow MHD}$ is the power transfer from fast ions to MHD modes within the corresponding flux surface. It can be seen from $P_{EP \rightarrow MHD}$ at $\psi/\psi_a = 1$ that net energy is transferred from fast ions to MHD modes in both cases. Here, the MHD modes are a core non-resonant $n = 1$ kink mode and a $(m, n) = (2, 1)$ NTM. The energy exchange is calculated using TRANSP for two mode amplitudes ($A/A_{meas} = 1$ and $A/A_{meas} = 2$) input to ORBIT. The sign convention is that when modes gain energy from fast ions, the power exchange is positive. When $A/A_{meas} = 1$, the MHD modes lose energy to fast ions only near the core. When $A/A_{meas} = 2$, the MHD modes lose energy to fast ions in the broader radial region including the $q = 2$ surface. That is, the energy exchange between the NTM and fast

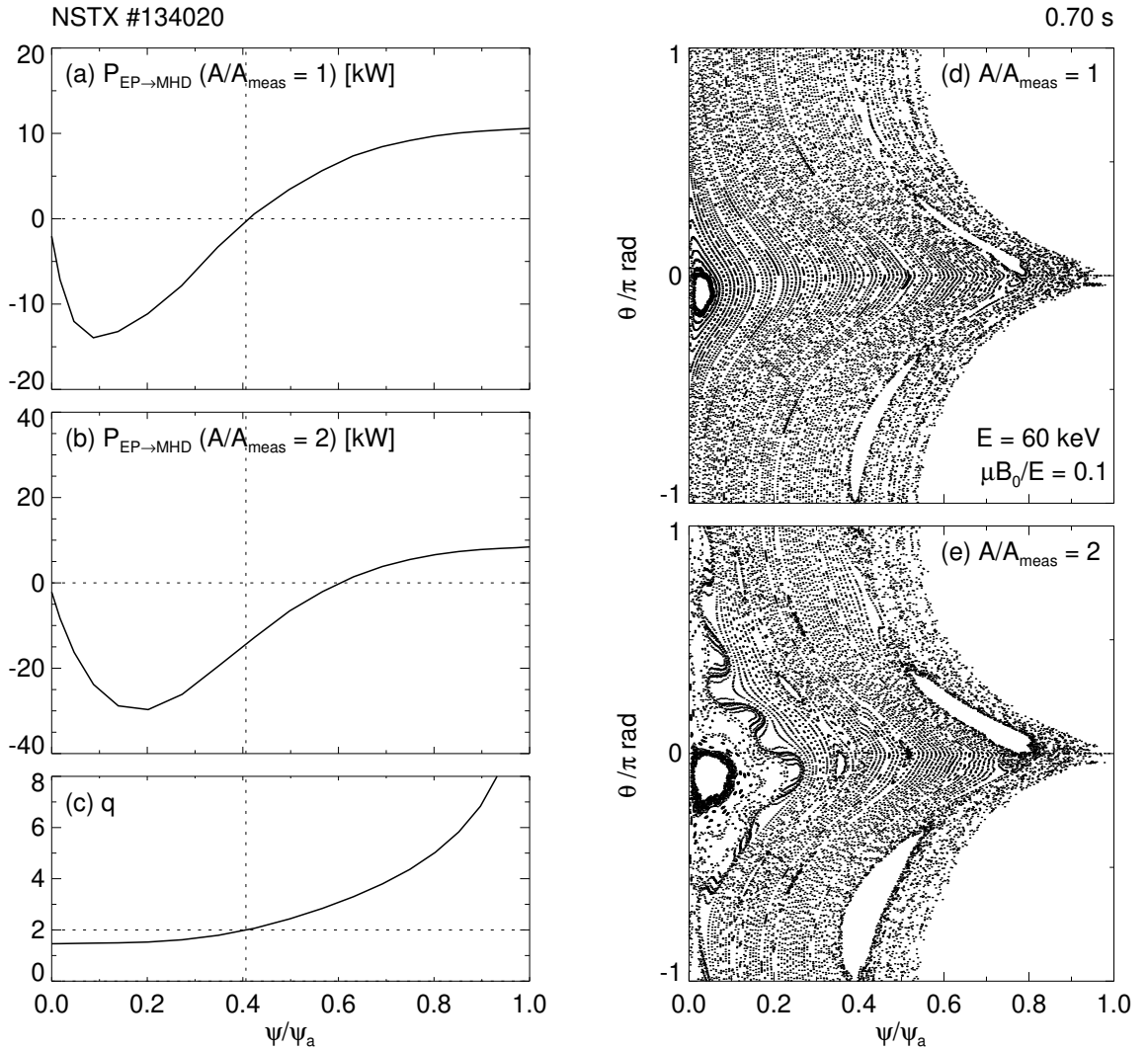


Figure 12. Profiles of energy exchange inside the flux surface from fast ion to modes for the case where mode amplitude is (a) the same, and (b) twice as measured mode amplitude, and (c) safety factor. Poincaré plots for the case where mode amplitude is (d) the same, and (e) twice as measured mode amplitude.

ions is not independent from that between the core kink mode and fast ions.

The Poincaré plots for each case discussed in the earlier paragraph are shown in Fig. 12 (d) and (e). It is known that stochasticity leads to increased fast ion transport, and that the “Chirikov criterion” where the stochasticity threshold is defined as the point where the last Kolmogorov-Arnold-Moser (KAM) surface disappears is a useful yet overestimating proxy. In fact, it was shown in DIII-D that fast ion transport starts to increase as the KAM surfaces start to break [46]. Fig. 12 (d) and (e) also shows that even when a plenty of KAM surfaces are observed at $A/A_{meas} = 2$, the fast ion loss can already be growing distinctively rapidly as shown in Fig. 11.

The broken KAM surfaces between the core and the $q = 2$ surface suggests a presence of a fast ion transport channel formed between the core and the $q = 2$ surface [4]. It can be suggested that the core kink mode and NTM are communicating with each other in terms of fast ion transport, and this may be the reason why a magnetic island stops growing when the orbits start to become stochastic and fast ion transport starts to increase rapidly in NSTX.

6. Conclusion and future work

The main result of this paper is that the “uncompensated cross field current” driven by fast ions allows for a small initial island to grow beyond the point where the polarization current stabilization is no longer effective, or to “open the gate” [25]. The predicted and measured time evolution of NTM island width is in good quantitative agreement when the prediction is based on the modified Rutherford equation only with the added fast ion term. The uncompensated cross field current can compete with the polarization current as suggested in [9]. This physical picture qualitatively explains another experimental observation that the measured island widths do not exceed the orbit stochasticization threshold: As island become larger, fast ions are lost due to orbit stochasticization, which leads to a weaker fast ion drive of NTM. In addition to the main result, we also report that a magnetic island may not necessarily be a “classical” tearing mode even if it grows like $w \sim t$, when the curvature term is sufficiently large as is often the case in spherical tori [28].

This work implies that a reliable and quantitative analysis of fast ion effect on NTM stability is possible with the self-consistent determination of relevant parameters using the TRANSP framework with the “kick” model [14]. We also note that the method of iterative fitting of the modified Rutherford equation coefficients using the island widths at time slices during mode excitation as constraints is applied successfully in the process of analysis. The improved prediction capability of modified Rutherford equation, both by the inclusion of correct terms into the equation and by the determination of coefficients for each terms, may provide a new insight on NTM onset and growth which is vital for an efficient NTM control in ITER and future devices.

In the future, our model will be improved. More discharges will be analyzed to create a database from which the modified Rutherford equation coefficients can be better constrained. The evaluation of classical stability index (Eq. 1), considering a single harmonic in the present form, will be benchmarked against the resistive stability code, STRIDE [47]. The effect of parallel current [8] will be included. The improved model will be compared to the first principle magnetohydrodynamic simulations including M3D-C¹ [48], which has a capability to handle multiple modes simultaneously that suits e.g. cases with the kink mode and NTM in NSTX. The improved model will also be compared to dedicated experiments in NSTX-U [49], which provides us with doubled magnetic field and a new tangential NB line.

Acknowledgment

The authors acknowledge Huishan Cai, Allan Reiman, and Chang Liu for their helpful suggestions. This manuscript is based upon work supported by the U.S. Department of Energy, Office of Science, Office of Fusion Energy Sciences, and has been authored by Princeton University under Contract Number DE-AC02-09CH11466 with the U.S. Department of Energy.

References

- [1] Chang Z and Callen J D 1990 *Nucl. Fusion* **30** 219
- [2] Zweben S J, Bush C E, Chang C S, Chang Z, Darrow D S, Fredrickson E D, Herrmann H W, Mynick H E, Schivell J, Bell M, Boivin R, Budny R V, Cheng C Z, Ernst D, Hammett G, Johnson L C, McCune D, Murakami M, Owens D K, Park J, Phillips C K, Redi M H, Scott S, Strachan J D, Taylor G, Tuszewski M, White R B, Wilson J R and Zarnstorff M 1994 *Phys. Plasmas* **1** 1469
- [3] Bardoczi L, Podestà M, Heidbrink W W and van Zeeland M A 2019 *Plasma Phys. Control. Fusion* **61** 055012
- [4] Yang J, Podestà M and Fredrickson E D 2021 *Plasma Phys. Control. Fusion* **63** 045003
- [5] Cai H 2021 *Nucl. Fusion* **61** 126012
- [6] Sesnic S, Gunter S, Gude A, Maraschek M and the ASDEX Upgrade Team 2000 *Phys. Plasmas* **7** 935
- [7] Fredrickson E D 2002 *Phys. Plasmas* **9** 548
- [8] Hegna C C and Bhattacharjee A 1989 *Phys. Rev. Lett.* **63** 2056
- [9] Cai H 2016 *Nucl. Fusion* **56** 126016
- [10] Heidbrink W W, Bardoczi L, Collins C S, Krammer G J, La Haye R J, Lin D J, Muscatello C M, Podestà M, Stagner L, Van Zeeland M A and Zhu Y B 2018 *Nucl. Fusion* **58** 082027
- [11] Chen W, Zhu X L, Wang F, Jiang M, Ji X Q, Qiu Z Y, Shi Z B, Yu D L, Li Y G, Yu L M, Shi P W, Ding X T, Xu M and Wang Z X 2019 *Nucl. Fusion* **59** 096037
- [12] Liu D, Heidbrink W W, Podestà M, Ren Z Z, Bardoczi L, Fredrickson E D, Fu G Y, Petty C C, Thome K E, Turco F and van Zeeland M A 2020 *Nucl. Fusion* **60** 112009
- [13] Poli F, Sachdev J, Breslau J, Gorelenkova M and Yuan X Transp (computer software) URL <https://dx.doi.org/10.11578/dc.20180627.4>
- [14] Podestà M, Gorelenkova M and White R B 2014 *Plasma Phys. Control. Fusion* **56** 055003
- [15] Fitzpatrick R 2016 *Phys. Plasmas* **23** 052506
- [16] Fredrickson E, Bell M, Budny R V and Synakowski E 2000 *Phys. Plasmas* **7** 4112
- [17] Rutherford P H 1973 *Phys. Fluids* **16** 1903
- [18] Furth H P, Killeen J and Rosenbluth M N 1963 *Phys. Fluids* **6** 459
- [19] Nave M F F and Wesson J A 1990 *Nucl. Fusion* **30** 2575
- [20] Fitzpatrick R 1995 *Phys. Plasmas* **2** 825
- [21] Gorelenkov N N, Budny R V, Chang Z, Gorelenkova M V and Zakharov L E 1996 *Phys. Plasmas* **3** 3379
- [22] Chang Z, Callen J D, Fredrickson E D, Budny R V, Hegna C C, McGuire K M, Zarnstorff M C and TFTR group 1995 *Phys. Rev. Lett.* **74** 4663
- [23] Wilson H R, Connor J W, Hastie R J and Hegna C C 1996 *Phys. Plasmas* **3** 248
- [24] Smolyakov A I, Hirose A, Lazzaro E, Re G B and Callen J D 1995 *Phys. Plasmas* **2** 1581
- [25] La Haye R J, Chrystal C, Strait E J, Callen J D, Hegna C C, Howell E, Okabayashi M and Wilcox R S 2022 *Nucl. Fusion* **62** 056017
- [26] La Haye R J 2006 *Phys. Plasmas* **13** 055501
- [27] Glasser A H, Greene J M and Johnson J L 1975 *Phys. Fluids* **18** 875

- [28] La Haye R J, Buttery R J, Gerhardt S P, Sabbagh S A and Brennan D P 2012 *Phys. Plasmas* **19** 062506
- [29] Kotschenreuther M, Hazeltine R D and Morrison P J 1985 *Phys. Fluids* **28** 294
- [30] Tang X, Lin Z, Heidbrink W W, Bao J, Xiao C, Li Z, Li J and Bardoczi L 2020 *Phys. Plasmas* **27** 032508
- [31] Mirnov V V, Ebrahimi F, Kim C C, King J R, Miller M C, Reusch J A, Sarff J S, Schnack D D, Sovinec C R and Tharp T D 2010 23rd int. fusion energy conf. *Proc. THS/P5-11* URL <http://www-naweb.iaea.org/napc/physics/FEC/FEC2010/html/fec10.htm>
- [32] Waelbroeck F L, Connor J W and Wilson H R 2001 *Phys. Rev. Lett.* **87** 215003
- [33] Ono M, Kaye S M, Peng Y K M, Barnes G, Blanchard W, Carter M D, Chrzanowski J, Dudek L, Ewig R, Gates D, Hatcher R E, Jarboe T, Jardin S C, Johnson D, Kaita R, Kalish M, Kessel C E, Kugel H W, Maingi R, Majeski R, Manickam J, McCormack B, Menard J, Mueller D, Nelson B A, Nelson B E, Neumeyer C, Oliaro G, Paoletti F, Parsells R, Perry E, Pomphrey N, Ramakrishnan S, Raman R, Rewoldt G, Robinson J, Roquemore A L, Ryan P, Sabbagh S, Swain D, Synakowski E J, Viola M, Williams M, Wilson J R and NSTX Team 2000 *Nucl. Fusion* **40** 557
- [34] LeBlanc B P 2008 *Rev. Sci. Instrum.* **79** 10E737
- [35] Bell R E, Andre R, Kaye S M, Kolesnikov R A, LeBlanc B P, Rewoldt G, Wang W X and Sabbagh S A 2010 *Phys. Plasmas* **17** 082507
- [36] Menard J E, Bell R E, Gates D A, Kaye S M, LeBlanc B P, Levinton F M, Medley S S, Sabbagh S A, Stutman D, Tritz K and Yuh H 2006 *Phys. Rev. Lett.* **97** 095002
- [37] Levinton F M and Yuh H 2008 *Rev. Sci. Instrum.* **79** 10F522
- [38] Gerhardt S P, Gates D A, Kaye S M, Maingi R, Menard J E, Sabbagh S A, Soukhanovskii V, Bell M G, Bell R E, Canik J M, Fredrickson E, Kaita R, Koleman E, Kugel H, Blanc B P L, Mastrovito D, Mueller D and Yuh H 2011 *Nucl. Fusion* **51** 073031
- [39] Podestà M, Gorelenkova M, Gorelenkov N N and White R B 2017 *Plasma Phys. Control. Fusion* **59** 055008
- [40] Goldston R J, McCune D C, Towner H H, Davis S L, Hawryluk R J and Schmidt G L 1981 *J. Comput. Phys.* **43** 61
- [41] White R B and Chance M S 1984 *Phys. Fluids* **27** 2455
- [42] Houlberg W A, Shaing K C, Hirshman S P and Zarnstorff M C 1997 *Phys. Plasmas* **4** 3230
- [43] Chang Z, Fredrickson E D, Batha S H, Bell M G, Budny R V, Levinton F M, McGuire K M, Taylor G, Zarnstorff M C and the TFTR Group 1998 *Phys. Plasmas* **5** 1076
- [44] Levenberg K 1944 *Quart. Appl. Math.* **2** 164
- [45] Halfmoon M R and Brennan D P 2017 *Phys. Plasmas* **24** 062501
- [46] Collins C S, Heidbrink W W, Austin M E, Kramer G J, Pace D C, Petty C C, Stagner L, van Zeeland M A, White R B, Zhu Y B and the DIII-D team 2016 *Phys. Rev. Lett.* **116** 095001
- [47] Glasser A and Koleman E 2018 *Phys. Plasmas* **25** 082502
- [48] Breslau J, Ferraro N and Jardin S 2009 *Phys. Plasmas* **16** 092503
- [49] Menard J E, Gerhardt S, Bell M, Bialek J, Brooks A, Canik J, Chrzanowski J, Denault M, Dudek L, Gates D A, Gorelenkov N, Guttenfelder W, Hatcher R, Hosea J, Kaita R, Kaye S, Kessel C, Koleman E, Kugel H, Maingi R, Mardenfeld M, Mueller D, Nelson B, Neumeyer C, Ono M, Perry E, Ramakrishnan R, Raman R, Ren Y, Sabbagh S, Smith M, Soukhanovskii V, Stevensen T, Strykowski R, Stutman D, Taylor G, Titus P, Tresemer K, Tritz K, Viola M, Williams M, Woolley R, Yuh H, Zhang H, Zhai Y, Zolfaghari A and the NSTX Team 2012 *Nucl. Fusion* **52** 083015